NASA TECHNICAL NOTE

NASA TN D-5108

NASA TN D-5108

EFFECTS OF BOTTOM-STRUCTURE FLEXIBILITY ON WATER LANDING LOADS OF APOLLO SPACECRAFT MODELS

by Sandy M. Stubbs and Melvin E. Hathaway

Langley Research Center
Langley Station, Hampton, Va.

NATIONAL AERONAUTICS AND SPACE ADMINISTRATION • WASHINGTON, D. C. • MARCH 1969

EFFECTS OF BOTTOM-STRUCTURE FLEXIBILITY ON WATER LANDING LOADS OF APOLLO SPACECRAFT MODELS

By Sandy M. Stubbs and Melvin E. Hathaway

Langley Research Center
Langley Station, Hampton, Va.

NATIONAL AERONAUTICS AND SPACE ADMINISTRATION

For sale by the Clearinghouse for Federal Scientific and Technical Information
Springfield, Virginia 22151 – CFSTI price $3.00

EFFECTS OF BOTTOM-STRUCTURE FLEXIBILITY ON WATER LANDING LOADS OF APOLLO SPACECRAFT MODELS

By Sandy M. Stubbs and Melvin E. Hathaway
Langley Research Center

SUMMARY

A landing investigation has been made to determine the effects of heat-shield flexibility on pressures and accelerations for water landings of Apollo spacecraft models. An additional purpose was to obtain accurate acceleration data on the landing impact of a spherical body in water for use in refinements of rigid-body analytical calculations. Two solid models and one flexible-bottom model were tested to determine impact pressures and accelerations. The flexible bottom was scaled in stiffness from an early Apollo heat-shield structural design. The test conditions were limited to symmetrical landing attitudes (0^{o}) without horizontal velocity in order to obtain pressure profiles and loads on the bottom surfaces of the models from a limited number of data channels. Two vertical velocities were used to determine the effect of velocity on the forces applied to the flexible bottom.

Good agreement was obtained between computed and experimental acceleration results for the solid models. Results from this investigation indicate that a virtual water mass factor of 0.9 should be used in computing impact forces for rigid spherical surfaces shaped like the Apollo aft heat shield. Pressure profiles were obtained from which forces and accelerations could be derived. The pressures, forces, and accelerations on the solid models vary approximately as the square of the velocity. The data from the solid models can be accurately converted to vehicles of other scales without major problems.

Maximum forces on the bottom surface of the particular flexible-bottom model used in this investigation were approximately 6700 lbf (30 kN) compared with maximum forces of 3800 lbf (17 kN) for the solid model for a landing velocity of 15 ft/sec (4.6 m/sec). Pressures, forces, and accelerations do not vary as the square of the velocity for flexible-bottom vehicles. The applied water forces on the bottom were changed substantially by the motions of the flexible structure; this indicates a significant interaction between the structural oscillations and water pressures.

INTRODUCTION

One of the many aspects of manned space flight being investigated by the National Aeronautics and Space Administration is the landing of a spacecraft upon its return to earth. Water landing investigations have been made with models of several different manned spacecraft and results from these investigations are presented in references 1 to 7. One reason for continued effort in this field is the possibility that maximum structural loads imposed on a spacecraft will occur during landing impact. The presently designed Apollo spacecraft has no impact attenuation system, and the elasticity of the flexible heat-shield structure may adversely affect the water landing loads.

Water pressure data, obtained from landings of a 1/4-scale model of the Apollo command module with a flexible bottom, are presented in reference 5 for a range of landing conditions consistent with parachute letdown. Because of a limited number of channels of instrumentation, only mean pressures over small sample panel areas were obtained.

The present investigation had two purposes: To determine the effect of structural flexibility on impact pressures and loads and to obtain accurate acceleration data on the landing impact of a spherical body in water for use in refinements of rigid-body analytical calculations. In order to determine the effects of flexibility, pressure distributions were obtained on a spherical surface (in this case representative of the Apollo aft heat-shield shape) for both a rigid body and for a body with a flexible bottom structure. To accomplish this with limited instrumentation it was necessary to restrict testing to a 90° flight path and a near 0° landing attitude.

The investigations were conducted in the Langley impacting structures facility.

The units used for the physical quantities defined in this paper are given in both U.S. Customary Units and in the International System of Units (SI). (See ref. 8.) Factors relating these two systems of units are presented in the appendix.

DESCRIPTION OF MODELS

Three models were used in this investigation. Model dimensions and configuration are given in figure 1 and are representative of 1/4-scale models of the Apollo command module. All the models had the same external geometry and were balanced to position the center of gravity along the center line (roll axis). The nature of the investigation eliminated the need for moment-of-inertia simulation.

One solid model (hereinafter designated model 1) had a mass of 5.72 slugs (83.5 kg) and was used exclusively for obtaining accurate acceleration data. The other solid model

(hereinafter designated model 2) had a mass of 5.14 slugs (75.0 kg) and was used to obtain both acceleration and pressure data. The third model, which was also 5.14 slugs (75.0 kg), had a solid upper body to which a flexible bottom was attached and is referred to subsequently as the flexible-bottom model. A sketch of the flexible-bottom model is presented in figure 2. This model was fabricated primarily from balsa wood with hardwood accelerometer mounts. The bottom surface, or simulated heat-shield structure, is shown in figure 3 and consisted of a core of styrene plastic foam sandwiched between two layers of fiber glass cloth impregnated with an epoxy resin. This bottom was similar to that described in references 5 and 9. It was attached to the upper body at a ring 14.38 inches (36.53 cm) in radius from the X-axis. The region of the model immediately above the bottom was vacant to provide clearance for pressure transducers and to allow for bottom motions. The aft bulkhead immediately above the heat-shield structure in the Apollo spacecraft was not simulated in this investigation.

The model bottom design furnished by an Apollo subcontractor was stated in reference 9 to be scaled for dynamic similarity, with EI/b (where E is modulus of elasticity, I is area moment of inertia, and b is the bottom characteristic length) scaled from an early spacecraft design. The mass distribution was simulated by distributing lead disks in the foam. The mass of the bottom was 0.65 slug (9.5 kg). A static load deflection curve for a bottom similar to the one used in this investigation is shown in reference 5. The bottom in reference 5 was tested to failure. The current bottom was statically loaded while fastened onto the model in the test configuration. The static load was 700 lbf (3.1 kN) (well below that required to produce any structural damage) and the deflection was 0.22 inch (0.56 cm).

Solid model 2 was similar to the flexible-bottom model. The major difference was that the bottom was bonded solidly to the balsa-wood upper body with no cavity behind the bottom. Solid model 1 was different from the other two models in that it was made mostly of pine wood. The bottom was not fiber glass-plastic foam, but the surface of the pine was covered by a thin layer of fiber glass for waterproofing. The data obtained from tests of the solid models may be converted to vehicles of other scales by the scale relationships presented in table I. These relationships, however, are not sufficient to scale data obtained with the flexible-bottom model.

INSTRUMENTATION AND TEST PROCEDURE

Instrumentation for the models during the landing test included accelerometers, pressure transducers, and displacement potentiometers, with attendant signal-conditioning and recording equipment. Characteristics of the particular instruments employed with each test model are presented in table II. The limiting frequency response for all instruments, except possibly the pressure transducers, was governed by the response of the

recording equipment which is also included in table II. The frequency response of the pressure transducers submerged in water was not known.

Special emphasis was given the instrumentation used with model 1. Each component of the instrumentation system (accelerometer, amplifier, and galvanometer) used on solid model 1 was first calibrated separately. The entire system was then calibrated by using galvanometer 1 (see table II) and was found to be accurate within ±2 percent from 0 to 600 hertz.

Two types of pressure transducers were used: A wire strain gage and a piezoelectric quartz crystal. Figure 4 is a sketch showing the location of the pressure transducers. The two piezoelectric pressure transducers were located near the center of the bottom close to the intended point of initial water contact and were used to determine whether the lower frequency strain-gage transducers were responding to the peak pressures. These transducers had a natural frequency in air of 130 kilohertz, but the response frequency in water was not known.

Care was taken in mounting all pressure transducers to obtain a flush mounting between the transducer and the bottom surface. The pressure transducers were affected by thermal shock upon impact with the cool water. To eliminate this shock and to obtain a watertight seal, thin plastic tape was placed over the transducers. It was determined that the tape did not affect the pressure values but acted only as a thermal insulator.

A linear potentiometer was used to measure the deflection (stroke) of the flexible bottom near its center.

The models were landed on a calm fresh-water landing surface at nominal impact velocities of 7.7 ft/sec (2.35 m/sec) and 15.2 ft/sec (4.63 m/sec). Horizontal velocity was zero. The models were landed with the symmetrical axis (X-axis) near vertical (0° pitch). It should be noted that the proposed Apollo spacecraft landing attitude relative to the water surface varies from -10° to -44° and does not include the more severe 0° attitude used in this investigation. A photograph of the test area showing the flexible-bottom model in the predrop position is shown in figure 5. The models were held in the predrop position by an aircraft bomb release. Gravity accelerated the models after release and the drop height was varied to produce the desired impact velocity. The time of free fall was measured and was used along with a local gravitational constant g of 32.15 ft/sec^2 (9.80 m/sec^2) to determine the impact velocity. The air drag on the vehicles was considered to have negligible effect on the velocity.

RESULTS AND DISCUSSION

The test conditions for the model impact landing in water are summarized in table III which also includes the measured maximum impact accelerations. These

accelerations, the pressures exerted on the bottom during impact, and the bottom deflection are discussed in the following sections.

Accelerations

Typical oscillograph records of acceleration time histories for model 1 are shown in figure 6. Indicated on these accelerometer traces are the fairings necessary to eliminate high-frequency structural oscillations. The maximum accelerations listed in table III(a) were obtained from these fairings. Several runs were made at the two impact velocities. There were small variations in the slopes of acceleration onset and variations in the magnitude of maximum acceleration. However, when all the data are averaged together (shown at the bottom of table III(a)), the results indicate that the maximum average accelerations vary as the square of the average impact velocity within 3 percent.

Figure 7 shows experimental acceleration time histories compared with results of a theoretical numerical integration procedure used for calculating acceleration time histories. The experimental curves were taken from the faired oscillograph records in figure 6. These two particular experimental curves were chosen because the maximum acceleration values were very close to the average maximum acceleration values of all the data (shown at the bottom of table III(a)).

The theoretical calculations are based on the principal of the conservation of momentum and the curves shown in figure 7 were obtained by using the procedure presented in reference 1 with the equations of motion modified to include the effect of gravity during impact. A water mass factor of 0.9 of the mass of a hemisphere of water whose diameter is the wetted diameter was used for the calculations presented herein instead of the factor 0.75 used in reference 1. The current experimental data were felt to be sufficiently accurate to permit the definition of a more specific water mass factor for the particular vehicle investigated. Several computations were made for a range of water mass factors and a factor of 0.9 was found to give the best agreement with all the experimental data.

Figure 8 shows typical oscillograph records for solid model 2 and the flexible-bottom model. The maximum accelerations listed in tables III(b) and (c) were obtained from fairings of the accelerometer traces. The acceleration time histories for the flexible-bottom model (fig. 8(b)) exhibit oscillations which are attributed to interaction of the water forces and bottom structural elasticity. This interaction results in maximum accelerations approximately double those measured on the solid models.

Pressures

Several runs were made with solid model 2 and the flexible-bottom model at velocities of both 7.5 ft/sec (2.3 m/sec) and 15 ft/sec (4.6 m/sec). In all runs the models

impacted the water surface at or near the axis of symmetry. Typical oscillograph records for both models are presented in figure 8 for only the 15 ft/sec (4.6 m/sec) velocity. Traces from the pressure transducers and the faired acceleration curve on solid model 2 (fig. 8(a)) are smoother than traces for the flexible-bottom model (fig. 8(b)). All the traces from the flexible-bottom model (fig. 8(b)) indicate bottom oscillations at approximately 100 hertz. For the flexible-bottom model all the instruments recorded negative values of pressure, acceleration, and bottom deflection. Some of the pressure transducers have negative values near 1 atmosphere (101 kN/m^2) for a short period in their time histories. The lower velocity runs, not shown, indicate the same trends.

Figure 9 is a plot of the maximum peak pressure values of each transducer as a function of the radial distance from the center of impact for solid and flexible-bottom models at both impact velocities. The flagged data points (fig. 9(a)) indicate that instrumentation response was attenuating the initial peak pressure values. Most of the unflagged data points shown at a distance of 0 to 2 inches (5 cm) from the center of impact were obtained from the piezoelectric pressure transducers with their higher frequency response capability. The solid line fairing disregards the flagged data points. The dashed curves in figures 9(a) and (b) were obtained by multiplying the low-velocity peak pressure curve by the ratio of the squares of the velocities. The close agreement between the dashed curve (fig. 9(a)) and the high-velocity curve indicates that pressures for the solid model vary as the square of the velocities. The curves in figure 9(b) indicate that the pressures generally do not vary as the square of the velocities for the flexible-bottom model. Furthermore, the peak pressure curves for the flexible-bottom model have a flat area and even a slight hump in contrast with the smooth peak pressure curves for the solid models. The maximum peak pressures for the flexible-bottom model were approximately 130 psi (900 kN/m^2) compared with a maximum peak pressure of approximately 280 psi (1900 kN/m^2) for the solid model at the higher velocity investigated. The differences in peak pressure values as well as the differences in shape of the curves are attributed to the modifications of the hydrodynamic loads by the motions of the flexible bottom.

Sample pressure profiles along the wetted radius which can be used to define the pressure distributions are shown in figure 10 for solid model 2 and the flexible-bottom model. The actual data readings were plotted and faired to obtain the lines shown. Typical data points are shown with their fairings for one profile on each model. Each profile shown was obtained when a particular pressure transducer reached its maximum value.

The pressure profiles shown in figure 10 are assumed to be the same along any radial line from the point of contact. It is felt that this assumption is valid because the impact is near the center of the model and no angular rotation is imparted to the model.

It should be noted that this assumption would not hold for an eccentric impact nor for an impact with horizontal velocity.

The braces in figure 10(a) indicate which pressure profiles occur near the time of maximum acceleration. The corresponding profiles for the flexible-bottom model are shown by the dashed line at a radial distance of 12.5 inches (31.8 cm). The significant point about the profiles shown in figure 10 is the smooth nature of the profiles for the solid model compared with the waving uneveness of the profiles for the flexible-bottom model. This uneveness and crossing of profiles indicates an oscillation in pressure at a given radial distance from the center of impact while the water line moves across the bottom. It is also interesting to note that on some profiles there are negative pressures over a major area of the bottom and that some of these pressures are approximately 1 atmosphere in magnitude. This is due to the water trying to separate from the bottom during a portion of each bottom oscillation.

Acceleration Time Histories Obtained From Pressure Data

Typical force time histories obtained from an area integration of the pressure profiles are shown in figure 11 for both models at the two velocities tested. The solid lines are the forces for solid model 2, and the dashed lines are the forces for the flexible-bottom model. Maximum measured forces on the bottom surface for the particular flexible-bottom model used in this investigation were approximately 6700 lbf (30 kN) compared with maximum forces of 3800 lbf (17 kN) for the solid model, for a landing velocity of 15 ft/sec (4.6 m/sec). Since these force curves were obtained directly from pressures on the bottom, independent of the accelerometers at the model center of gravity, the differences in the solid and dashed curves are caused by the flexibility of the model bottom. This flexibility creates an interaction between the applied load and the local motions of the bottom.

The force time histories in figure 11 were converted to acceleration (g units) by dividing them by the model weight (mass $\times$ gravitational constant) and this acceleration time history obtained from pressure data is presented in figures 12 and 13 along with acceleration time histories taken from accelerometers mounted to the upper body at the model center of gravity. Close agreement is shown in these figures between the acceleration of the model obtained from the pressures or forces, and the acceleration measured with an accelerometer at the model center of gravity. Calculated rigid-body accelerations are also shown for comparison purposes in figures 12(a) and 13(a). In the calculations the water mass factor 0.9 discussed previously was used. Good agreement was obtained between the calculated curves and the experimental curves.

The maximum acceleration values shown in figures 12(a) and 13(a) for solid model 2 vary approximately as the square of the impact velocity as did the maximum pressure

values in figure 9(a) discussed previously. For the flexible-bottom model used in this investigation, the maximum acceleration values also seem to vary as the square of the impact velocities. It is thought that this is a feature of the particular model used in the investigation and would not be common to other structures or other test vehicles since other parts of the force and acceleration time histories do not vary as the square of the velocities. For example, the negative acceleration and force values found for the 15 ft/sec (4.6 m/sec) landing velocity do not show up for the 7.73 ft/sec (2.36 m/sec) landing velocity. This is supported by the data shown in figure 9(b) which indicate that the maximum pressure values for the flexible-bottom model do not vary as the velocity squared.

For the sake of completeness, bottom deflections are shown in figures 12(b) and 13(b) for comparison with the acceleration data.

Interaction Effects

Prior to this investigation accelerations measured at the model center of gravity were generally assumed to be a result of the structural response to a rigid-body applied load. A coupled phenomenon which causes a change in the applied load itself due to interaction of the structural oscillations and the water was considered relatively unimportant. By obtaining measured pressure values on the flexible bottom and converting them to force and acceleration values, it is shown that the applied load is changed substantially by the flexibility of the bottom; thus interaction is indicated. A theoretical approach to this type of interaction problem is presented in references 10 and 11. A comparison of results from these references and the present investigation indicate qualitative agreement. In addition, unpublished experimental data have been obtained at NASA's Manned Spacecraft Center, in which the interaction effect was investigated by using accelerometers on the bottom itself. Results from that investigation confirm the findings presented in this paper. It should be noted that a vehicle with different elastic characteristics would quite likely experience interaction, but predicting the magnitude of the pressure and force values or the frequency of bottom oscillation for a different structure might be difficult. It should be further pointed out that the scale relationships presented in table I are not sufficient if any attempt is made at extrapolating this data to vehicles of other sizes or with different structural characteristics. The data indicate that the Apollo spacecraft bottom, if it is sufficiently flexible, may be subjected to higher forces in a water landing mode than those predicted by rigid-body theory or rigid-body experiments. However, since the Apollo spacecraft is not intended to land at an attitude of 0^{o} as in this investigation, the magnitude of the increased forces in a normal landing may not be as severe as the data in this report indicate.

CONCLUDING REMARKS

A landing investigation has been made to determine the effects of heat shield flexibility on pressures and accelerations for water landings of both solid and flexible-bottom Apollo spacecraft models. An additional purpose was to obtain accurate acceleration data on the landing impact of a spherical body in water for use in refinements of rigid-body analytical calculations. Good agreement was obtained between computed and experimental acceleration results for a solid model. Results from this investigation indicate that a virtual water mass factor of 0.9 should be used in computing impact forces for rigid spherical surfaces shaped like the Apollo aft heat shield. Pressure profiles were obtained from which forces and accelerations could be derived. The pressures and accelerations on the solid model vary approximately as the square of the velocity.

Maximum forces on the bottom surface for the particular flexible-bottom model used in this investigation were approximately 6700 lbf (30 kN) compared with maximum forces of 3800 lbf (17 kN) for the solid model, for a landing velocity of 15 ft/sec (4.6 m/sec). Pressures, forces, and accelerations do not necessarily vary as the square of the velocity for flexible-bottom vehicles. The applied water forces on the bottom were changed substantially by the motions of the flexible structure; this indicates a significant interaction between the structural oscillations and the water pressures.

Langley Research Center,
National Aeronautics and Space Administration,
Langley Station, Hampton, Va., January 21, 1969,
124-08-04-06-23.

APPENDIX

CONVERSION OF U.S. CUSTOMARY UNITS TO SI UNITS

The International System of Units (SI) was adopted by the Eleventh General Conference on Weights and Measures, Paris, October 1960 (ref. 8). Conversion factors for the units used herein are given in the following table:

Physical quantity	U.S. Customary Unit	Conversion factor (*)	SI Unit
Length	in.	0.0254	meters (m)
Area	in^2	6.4516×10^{-4}	$meters^2$ (m^2)
Mass	slug	14.5939	kilograms (kg)
Velocity	ft/sec	0.3048	meters/second (m/sec)
Linear acceleration	ft/sec^2	0.3048	$meters/second^2$ (m/sec^2)
Force	lbf	4.448	newtons (N)
Pressure	lbf/in^2	6.895×10^3	$newtons/meter^2$ (N/m^2)

*Multiply value given in U.S. Customary Unit by conversion factor to obtain equivalent value in SI Unit.

Prefixes to indicate multiples of units are as follows:

Prefix	Multiple
milli (m)	10^{-3}
centi (c)	10^{-2}
kilo (k)	10^3

REFERENCES

1. McGehee, John R.; Hathaway, Melvin E.; and Vaughan, Victor L., Jr.: Water-Landing Characteristics of a Reentry Capsule. NASA MEMO 5-23-59L, 1959.

2. Vaughan, Victor L., Jr.: Landing Characteristics and Flotation Properties of a Reentry Capsule. NASA TN D-653, 1961.

3. Thompson, William C.: Dynamic Model Investigation of the Landing Characteristics of a Manned Spacecraft. NASA TN D-2497, 1965.

4. Stubbs, Sandy M.: Landing Characteristics of the Apollo Spacecraft With Deployed-Heat-Shield Impact Attenuation Systems. NASA TN D-3059, 1966.

5. Stubbs, Sandy M.: Dynamic Model Investigation of Water Pressures and Accelerations Encountered During Landings of the Apollo Spacecraft. NASA TN D-3980, 1967.

6. Stubbs, Sandy M.: Water Pressures and Accelerations During Landing of a Dynamic Model of the Apollo Spacecraft With a Deployed-Heat-Shield Impact-Attenuation System. NASA TN D-4275, 1968.

7. Thompson, William C.: Dynamic Model Investigation of the Rough-Water Landing Characteristics of a Spacecraft. NASA TN D-3774, 1967.

8. Comm. on Metric Pract.: ASTM Metric Practice Guide. NBS Handbook 102, U.S. Dep. Com., Mar. 10, 1967.

9. Bennett, R. V.; and Koerner, F. W.: 1/4 Scale Apollo Impact Attenuation Model. Rept. No. Na62H-513, North Am. Aviation, Inc., Sept. 14, 1962.

10. Wilkinson, J. P. D.; Capelli, A. P.; and Salzman, R. N.: Study of Apollo Water Impact. Volume 3: Dynamic Response of Shells of Revolution During Vertical Impact Into Water – Hydroelastic Interaction. SID 67-498 (Contract NAS9-4552), N. Amer. Aviat., Inc., May 1967.

11. Bingman, Ralph N.: Water Impact Loads on Structures. GAM/MECH 67-1, Air Force Inst. of Technol., May 1967.

TABLE I.- SCALE RELATIONSHIPS FOR USE IN OBTAINING LARGER OR SMALLER MODELS OF THE SOLID MODELS USED IN THIS INVESTIGATION

[λ = Scale of model]

Solid model dimension	Scale factor
Length, l	λ
Area, A	λ^2
Mass, m	λ^3
Time, t	$\sqrt{\lambda}$
Velocity, v	$\sqrt{\lambda}$
Linear acceleration, a	1
Force, F	λ^3
Pressure, p	λ

TABLE II.- INSTRUMENTATION CHARACTERISTICS

(a) Solid model 1

Accelerometer type	Accelerometer orientation	Range, g units	Flat frequency response	Limiting flat frequency of other recording equipment
Piezo-resistive strain gage	Normal on X-axis	±250	<±1% (0 to 500 Hz) ±5% (0 to 700 Hz)	Galvanometer 1, ±2% (0 to 600 Hz) Galvanometer 2, ±2% (0 to 190 Hz)

(b) Solid model 2

Accelerometer type	Accelerometer orientation	Range, g units	Flat frequency response	Limiting flat frequency of other recording equipment
Wire strain gage	Normal on X-axis	±50	±5% (0 to 450 Hz)	±5% (0 to 600 Hz)

Pressure transducer		Range		Approximate natural frequency in air, kHz	Limiting flat frequency of other recording equipment
Type	Number	psi	kN/m^2		
Wire strain gage	1	150	1 030	12	±5% (0 to 5 kHz)
	2	150	1 030	12	
	3	150	1 030	12	
	4	100	690	11	
	5	150	1 030	12	
	6	100	690	11	
	7	100	690	11	
	8	150	1 030	17	
	9	100	690	15	
	10	100	690	15	
	11	75	520	13	
	12	75	520	13	
	13	100	690	11	
	14	100	690	11	
	15	100	690	11	
	16	100	690	11	
	17	100	690	11	
	18	100	690	11	
Piezoelectric quartz crystal	19	15 000	103 000	130	±5% (0 to 20 kHz)
	20	15 000	103 000	130	

(c) Flexible-bottom model

Accelerometer type	Accelerometer orientation	Range, g units	Flat frequency response	Limiting flat frequency of other recording equipment
Wire strain gage	Normal on X-axis	±50	±5% (0 to 450 Hz)	±5% (0 to 180 Hz)
Piezoresistive strain gage	Normal on X-axis	±250	<±1% (0 to 500 Hz)	±5% (0 to 180 Hz)

Pressure transducer		Range		Approximate natural frequency in air, kHz	Limiting flat frequency of other recording equipment
Type	Number	psi	kN/m^2		
Wire strain gage	1	250	1 720	14	±5% (0 to 5 kHz)
	2	150	1 030	12	
	3	200	1 380	13	
	4	200	1 380	13	
	5	150	1 030	12	
	6	100	690	11	
	7	100	690	11	
	8	150	1 030	17	
	9	100	690	15	
	10	100	690	15	
	11	75	520	13	
	12	75	520	13	
	13	100	690	11	
	14	100	690	11	
	15	100	690	11	
	16	200	1 380	13	
	17	100	690	11	
	18	100	690	11	
Piezoelectric quartz crystal	19	15 000	103 000	130	±5% (0 to 24 kHz)
	20	15 000	103 000	130	

Linear potentiometer measuring	Approximate range		Limiting flat frequency of other recording equipment
	in.	cm	
Bottom deflection	6.0	15	±5% (0 to 360 Hz)

TABLE III.- MAXIMUM ACCELERATION DATA

(a) Solid model 1

[Horizontal velocity, 0; pitch, roll, and yaw, 0°]

	Vertical velocity		Normal acceleration measured from zero g (free fall), g units
	ft/sec	m/sec	
Frequency response, 600 Hz	7.81	2.38	5.7
	7.76	2.37	5.4
	7.67	2.34	5.7
	7.73	2.36	5.5
	15.2	4.63	22.1
	15.2	4.63	21.0
	15.2	4.63	19.1
Frequency response, 190 Hz	7.68	2.34	5.5
	7.71	2.35	5.5
	7.75	2.36	5.5
	15.2	4.63	20.4
	15.2	4.63	21.4
	15.2	4.63	21.1
Low-velocity average	7.73	2.36	5.6
High-velocity average	15.2	4.63	20.8

(b) Solid model 2

[Horizontal velocity, 0; roll attitude, 0°]

Vertical velocity		Run	Pitch	Yaw	Normal acceleration measured from zero g (free fall), g units
ft/sec	m/sec				
7.62	2.32	1	0°	0°	5.9
7.59	2.31	2	0°	0°	5.5
7.60	2.32	3	0°	0°	5.3
15.32	4.67	4	-1°	Right 1°	21.0
15.29	4.66	5	-1°	Right 1°	22.3
15.33	4.67	6	-2°	Right 2°	18.7

(c) Flexible-bottom model

[Horizontal velocity, 0; roll attitude, 0°]

Vertical velocity		Run	Pitch	Yaw	Normal acceleration measured from zero g (free fall), g units		Bottom deflection	
ft/sec	m/sec				50g accelerometer	250g accelerometer	in.	cm
7.73	2.36	1	0°	0°	10.8	10.3	0.13	0.33
7.57	2.31	2	0°	0°	10.9	10.4	.11	.28
7.59	2.31	3	0°	0°	11.1	9.9	.11	.28
15.08	4.60	4	0°	0°	40.0	41.3	.40	1.02
15.11	4.61	5	-2°	0°	43.5	41.3	.39	.99
15.09	4.60	6	0°	0°	43.8	40.4	.40	1.02

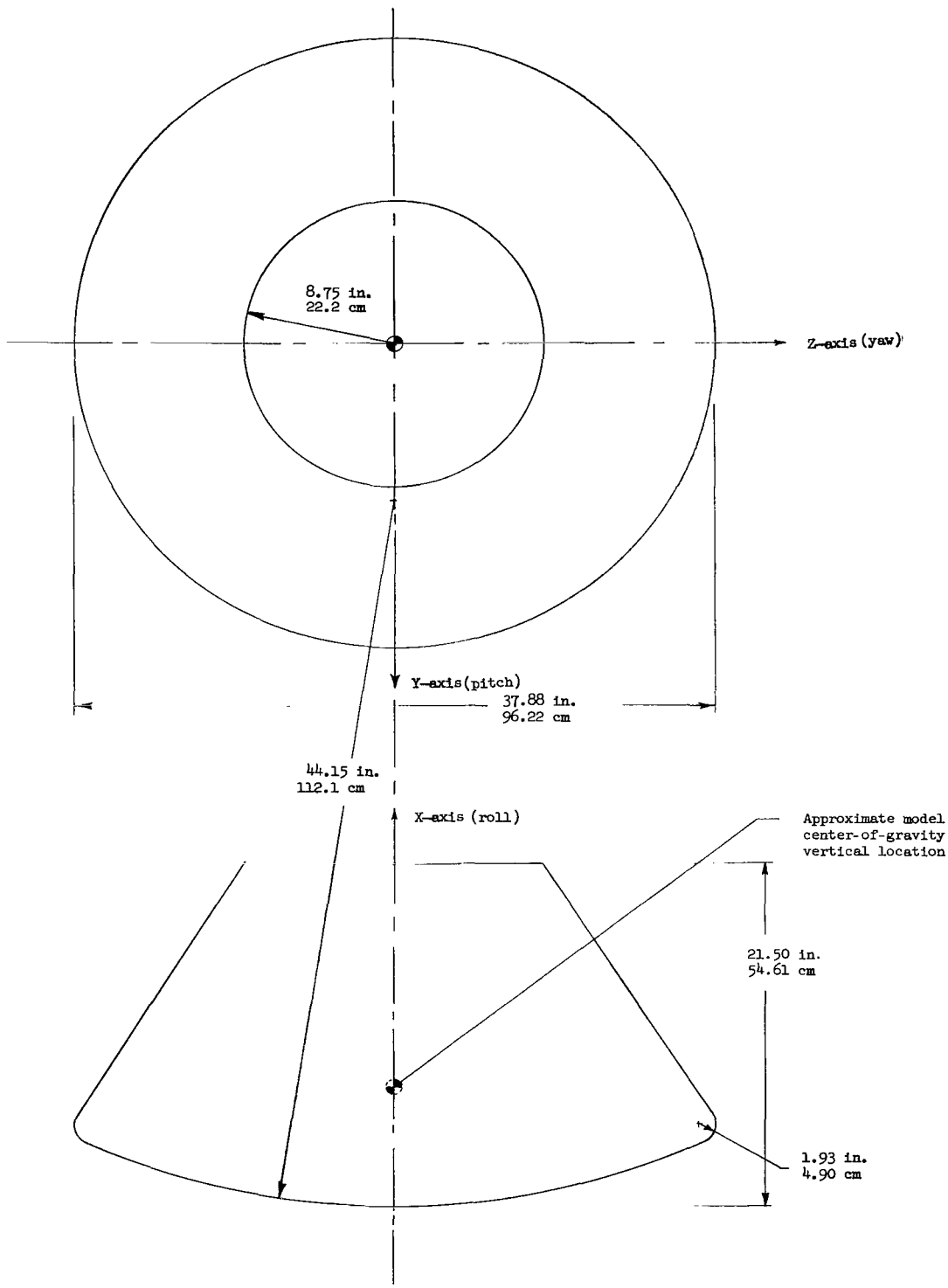

Figure 1.- Model configuration.

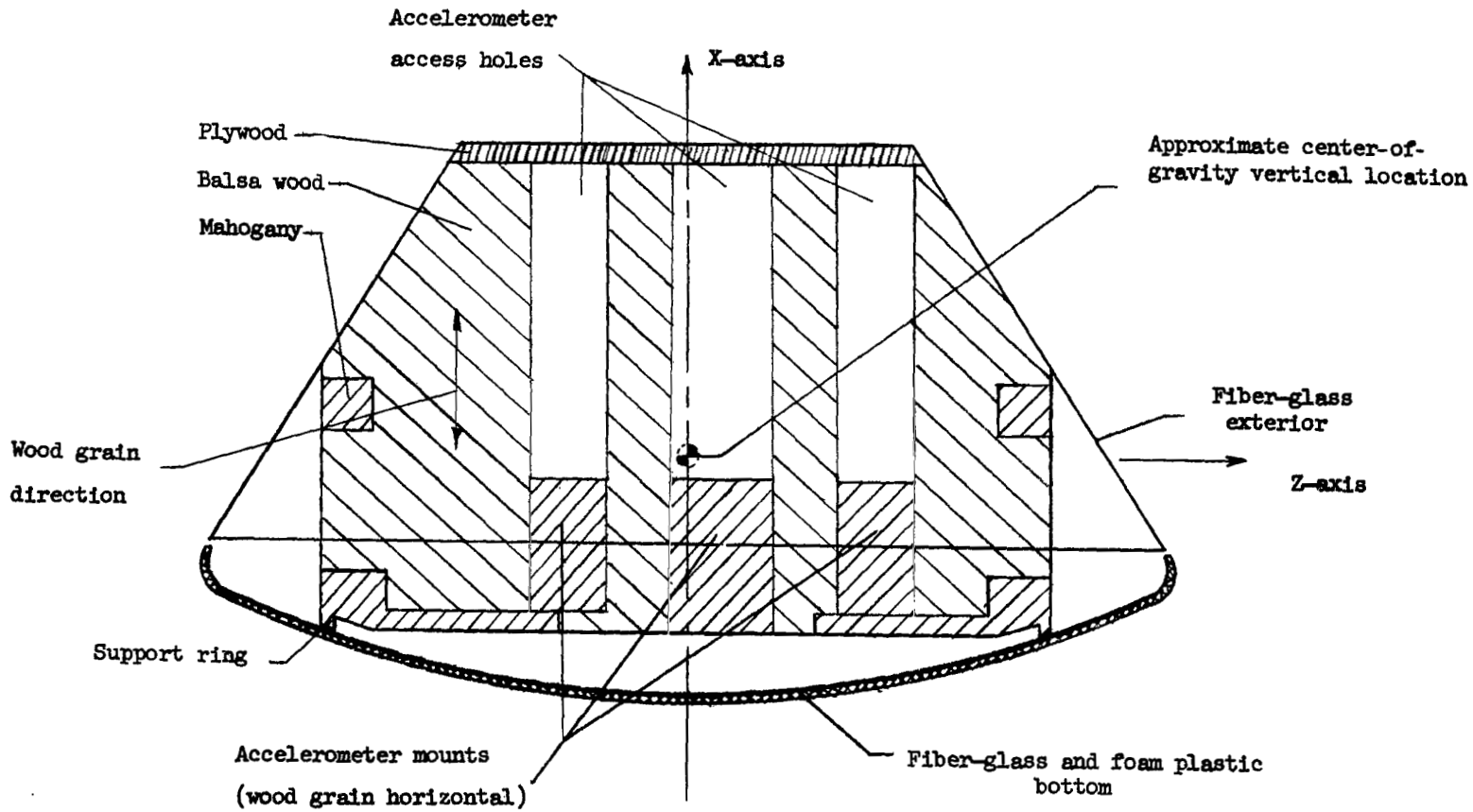

Figure 2.- Cross section of flexible-bottom model showing construction details.

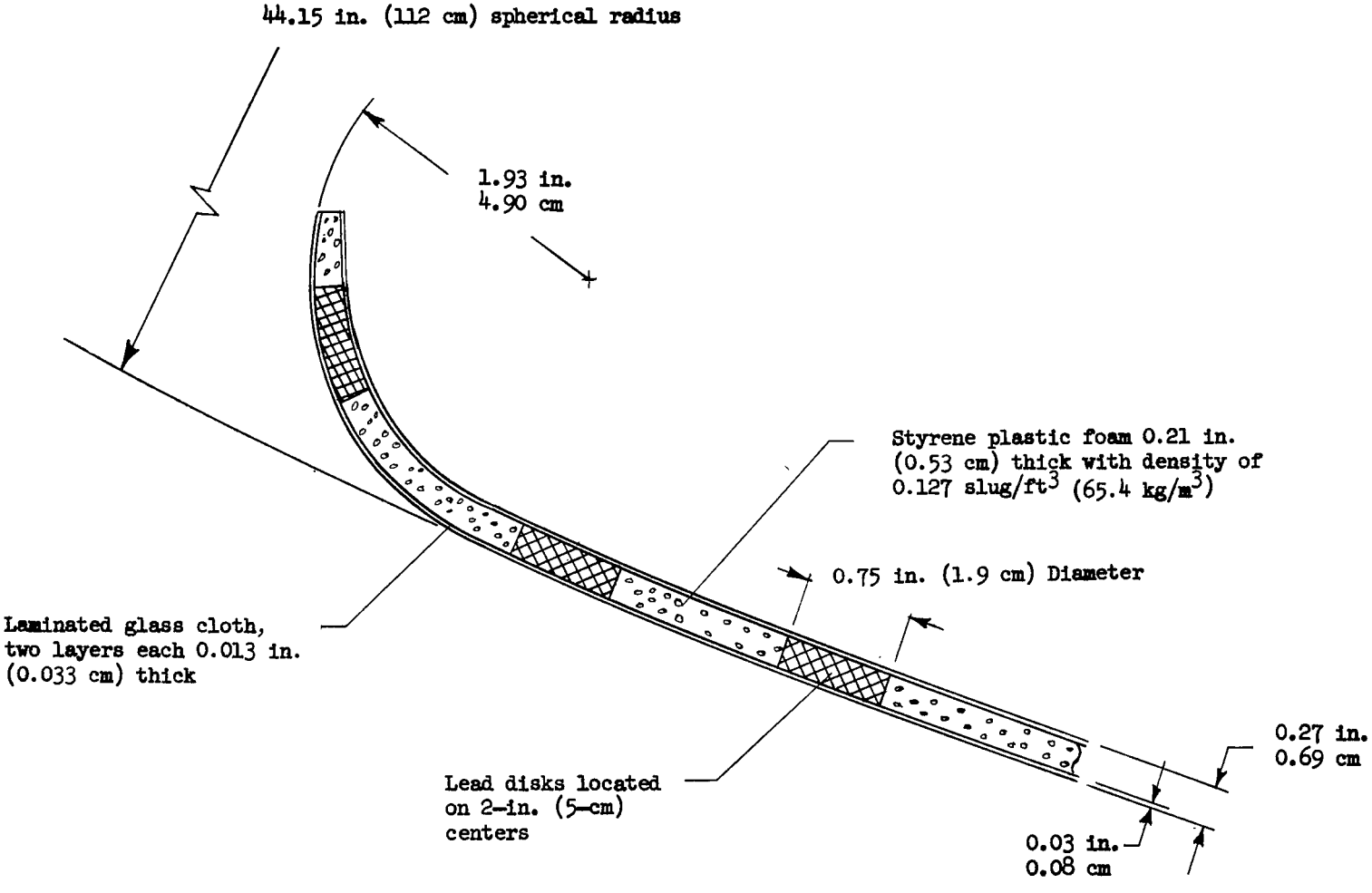

Figure 3.- Construction details of flexible bottom.

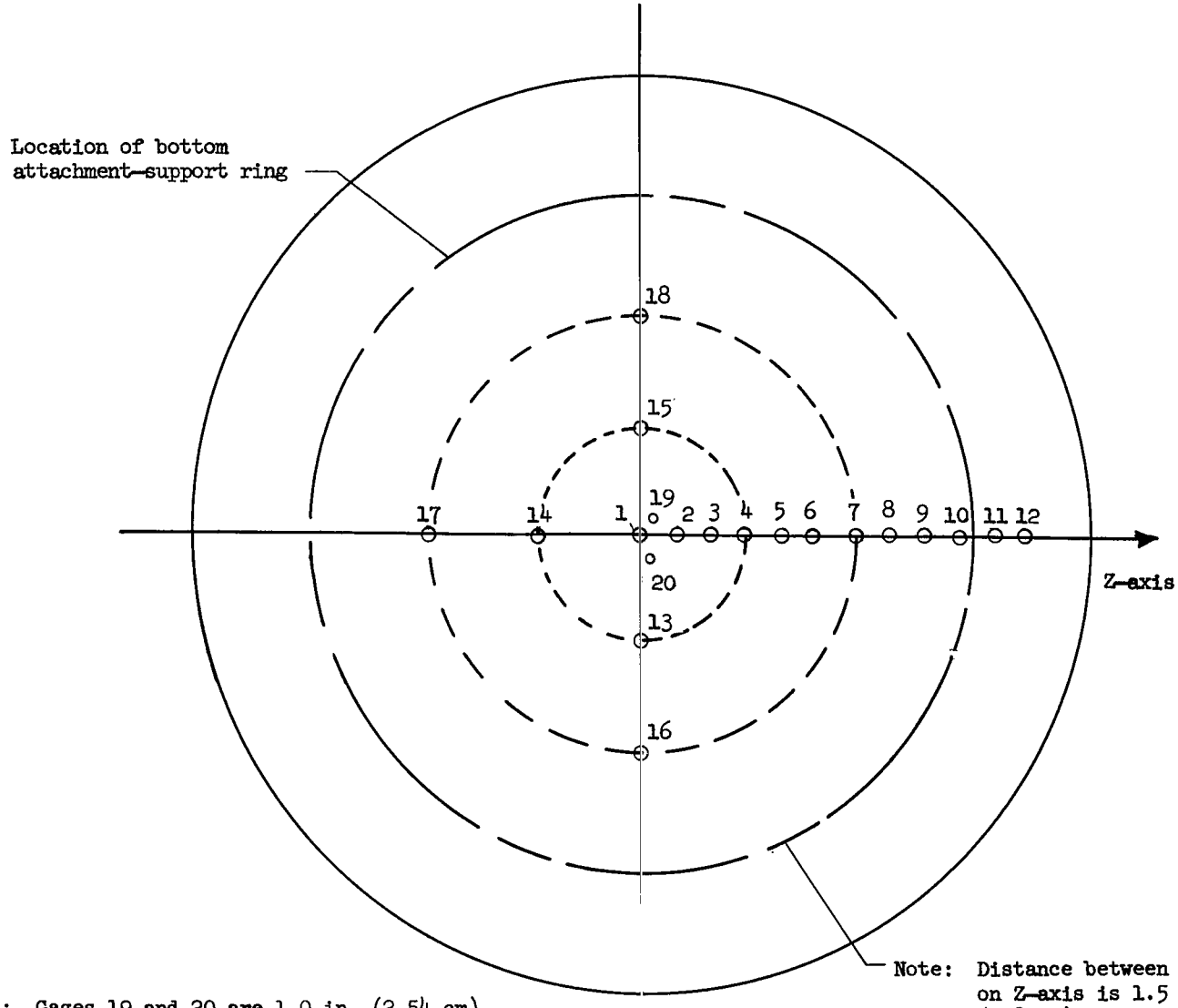

Figure 4.- Sketch showing locations of pressure transducers.

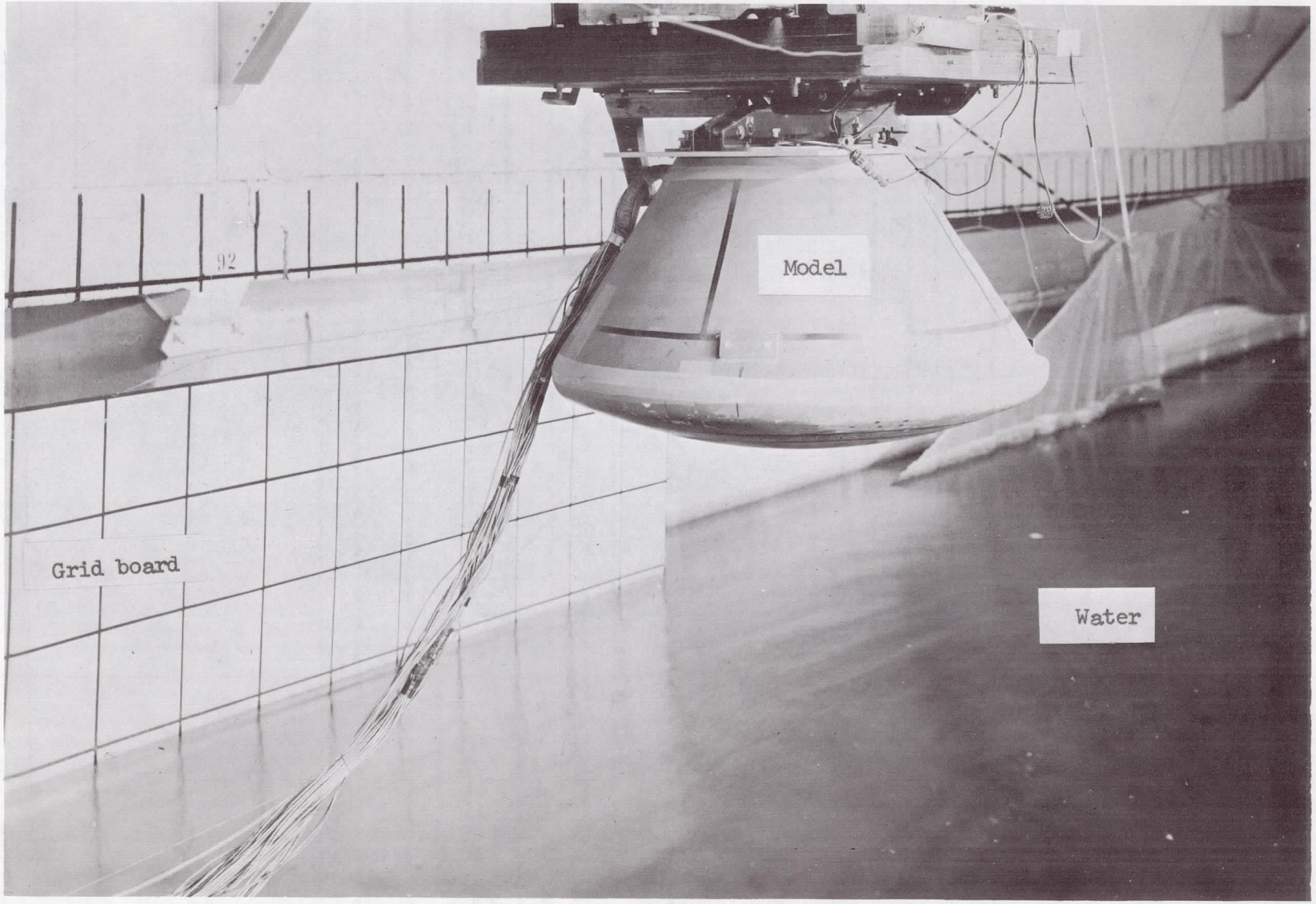

Figure 5.- Test area setup showing model at predrop position.

L-68-10,100

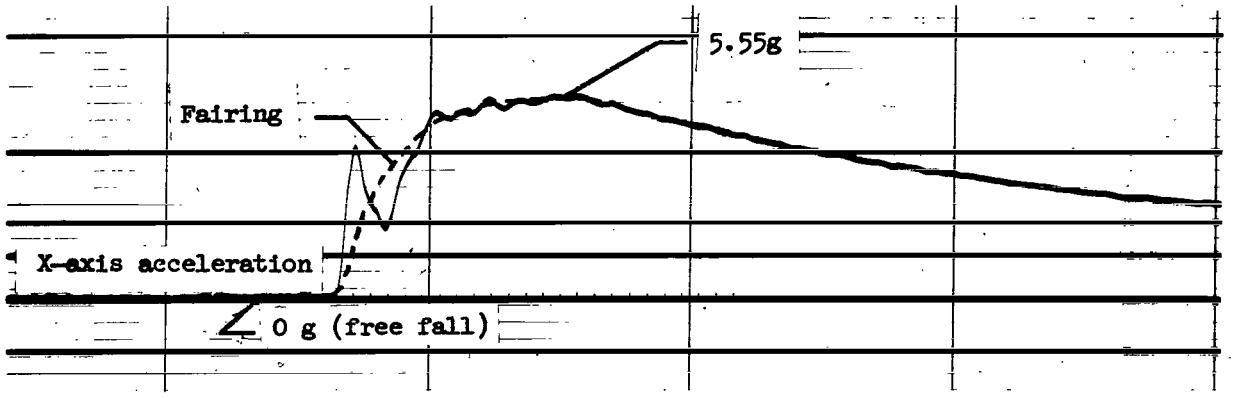

(a) Vertical velocity, 7.75 ft/sec (2.36 m/sec); flat frequency response, 190 Hz.

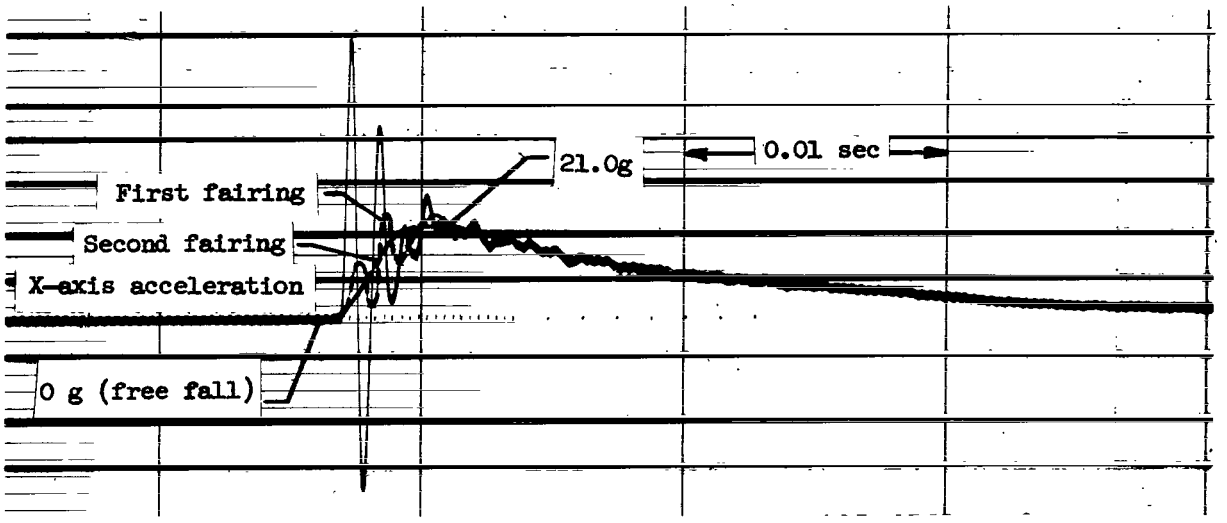

(b) Vertical velocity, 15.2 ft/sec (4.63 m/sec); flat frequency response, 600 Hz.

Figure 6.- Typical oscillograph records for solid model 1. Horizontal velocity, 0.

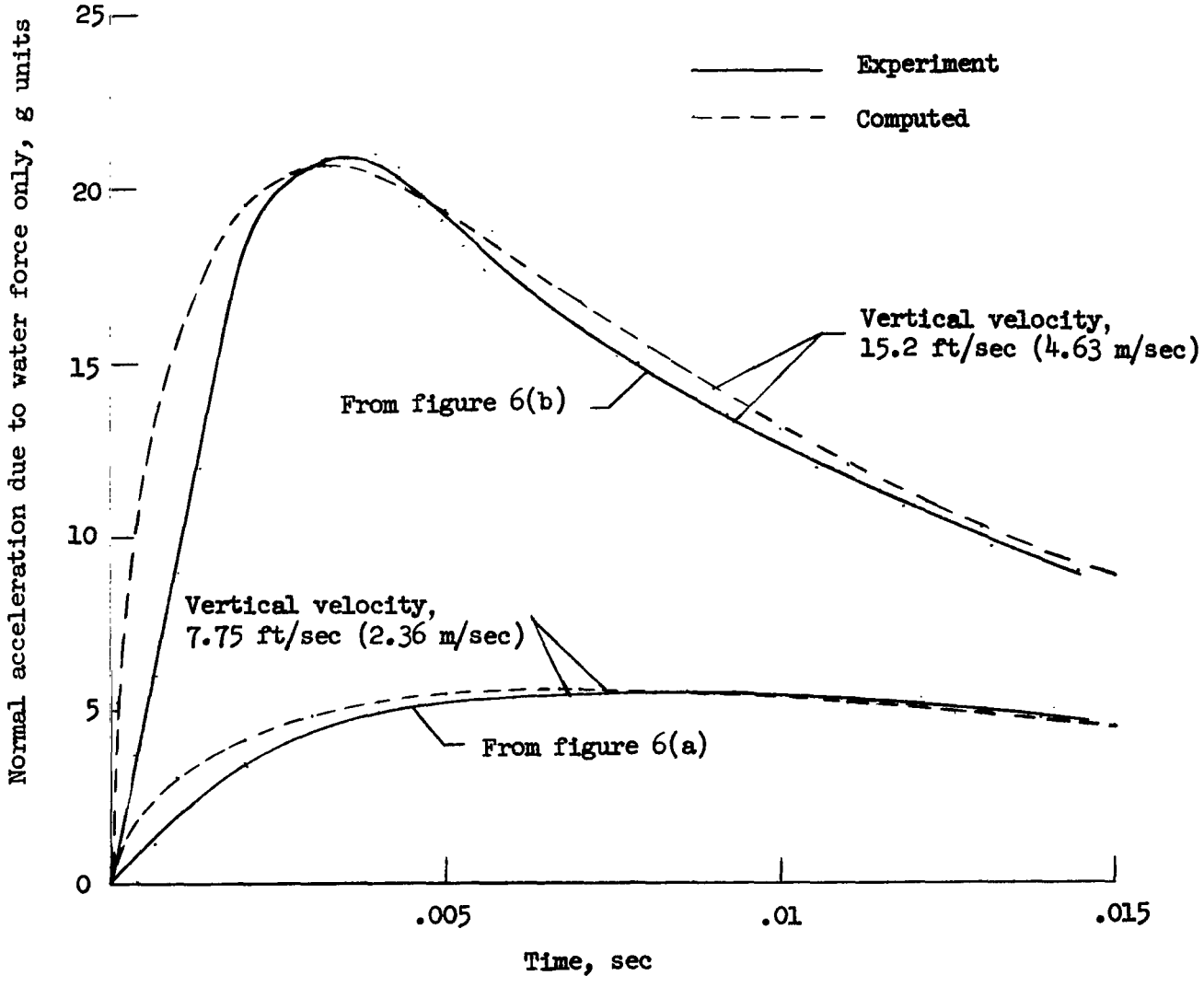

Figure 7.- Comparison of experimental acceleration time histories with theoretical results for solid model 1.

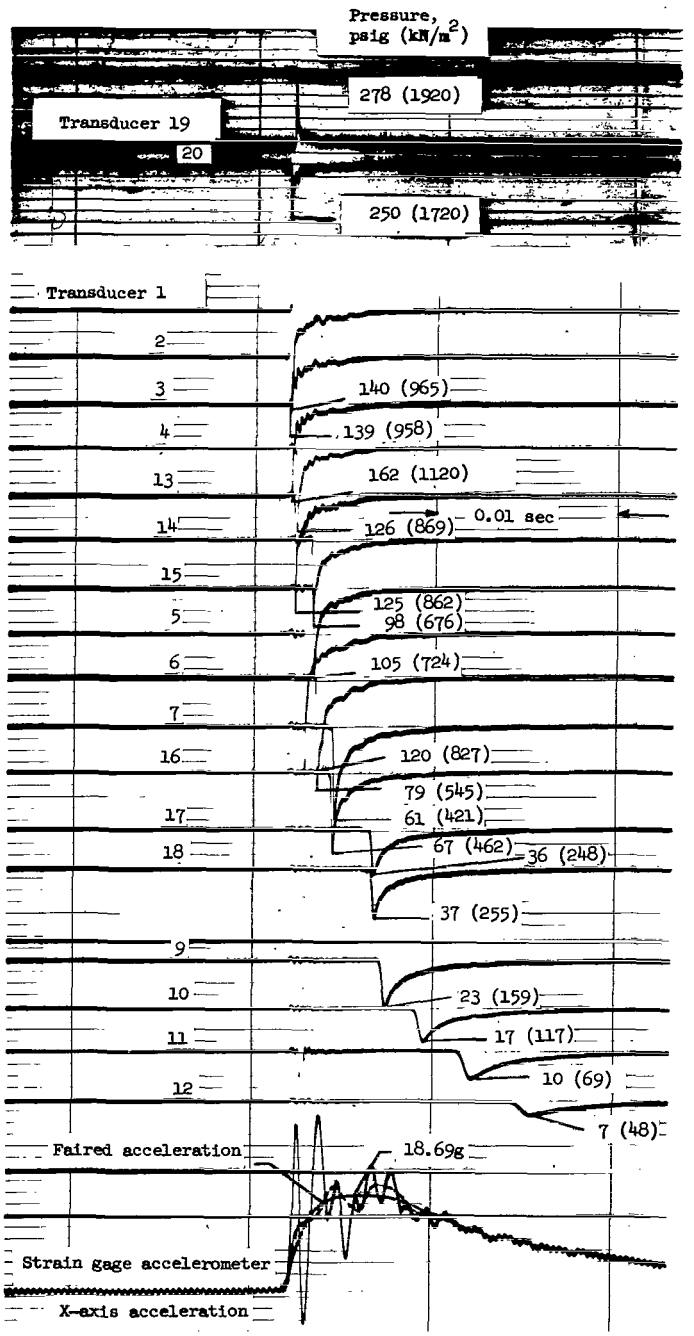

(a) Solid model 2. Run 6; vertical velocity, 15.33 ft/sec (4.67 m/sec).

Figure 8.- Typical oscillograph records of accelerations, pressures, and deflection for solid model 2 and flexible-bottom model. Initial pressure values are in psig; parenthetical values are in kN/m^2.

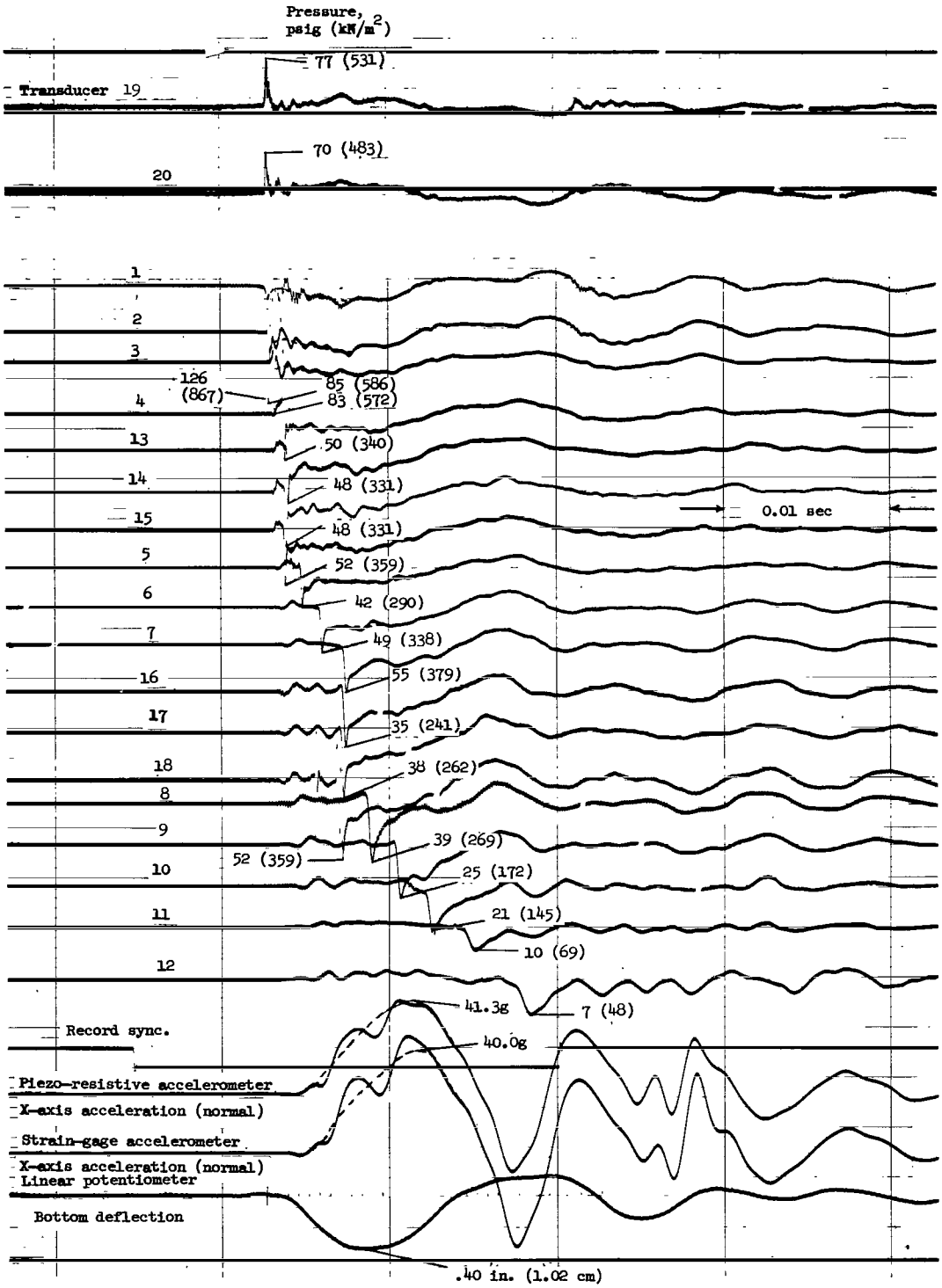

(b) Flexible-bottom model. Run 4; vertical velocity, 15.08 ft/sec (4.60 m/sec).

Figure 8.- Concluded.

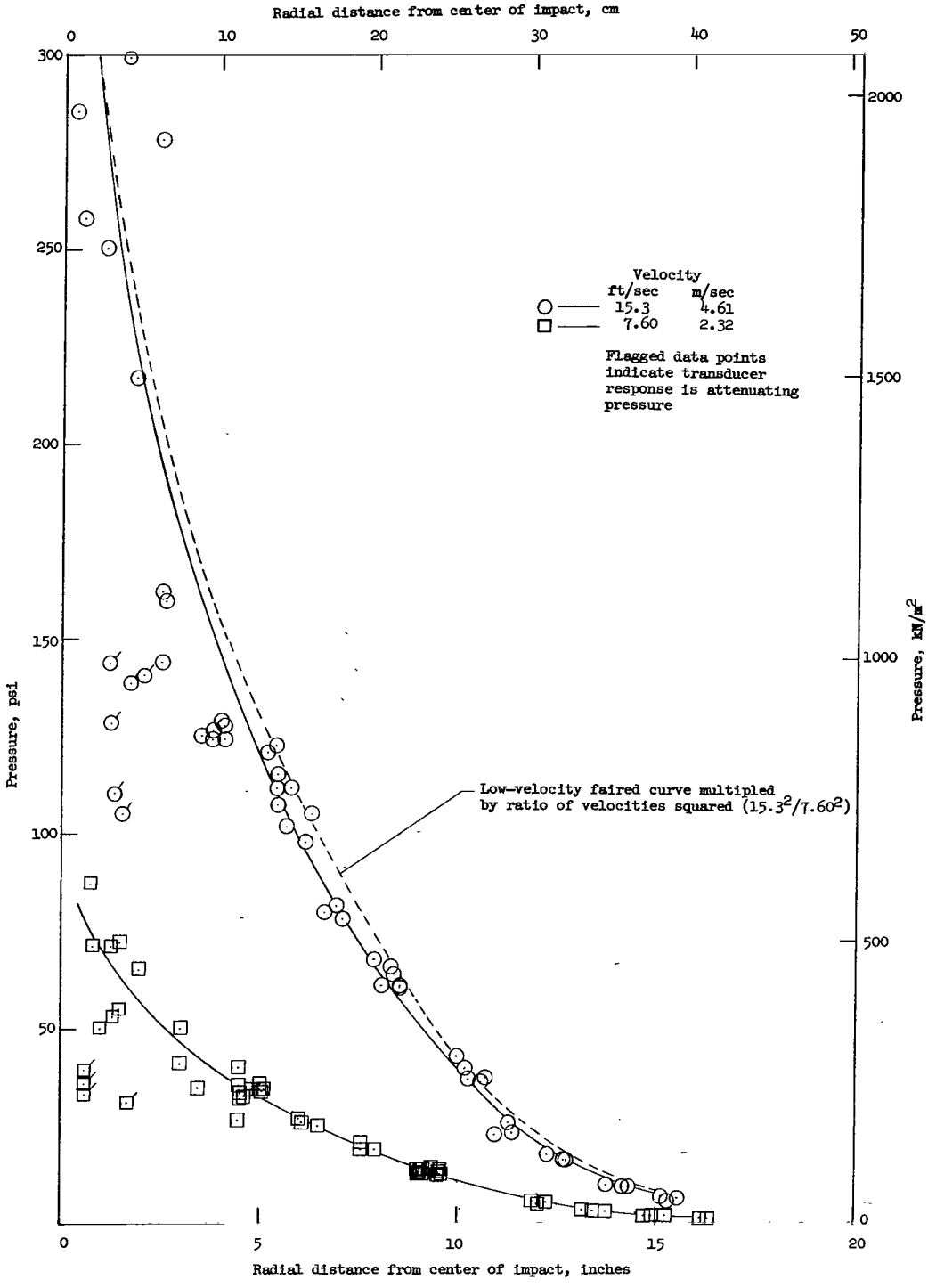

(a) Solid model 2.

Figure 9.- Maximum peak pressures of transducers. Data presented are from all runs of each model.

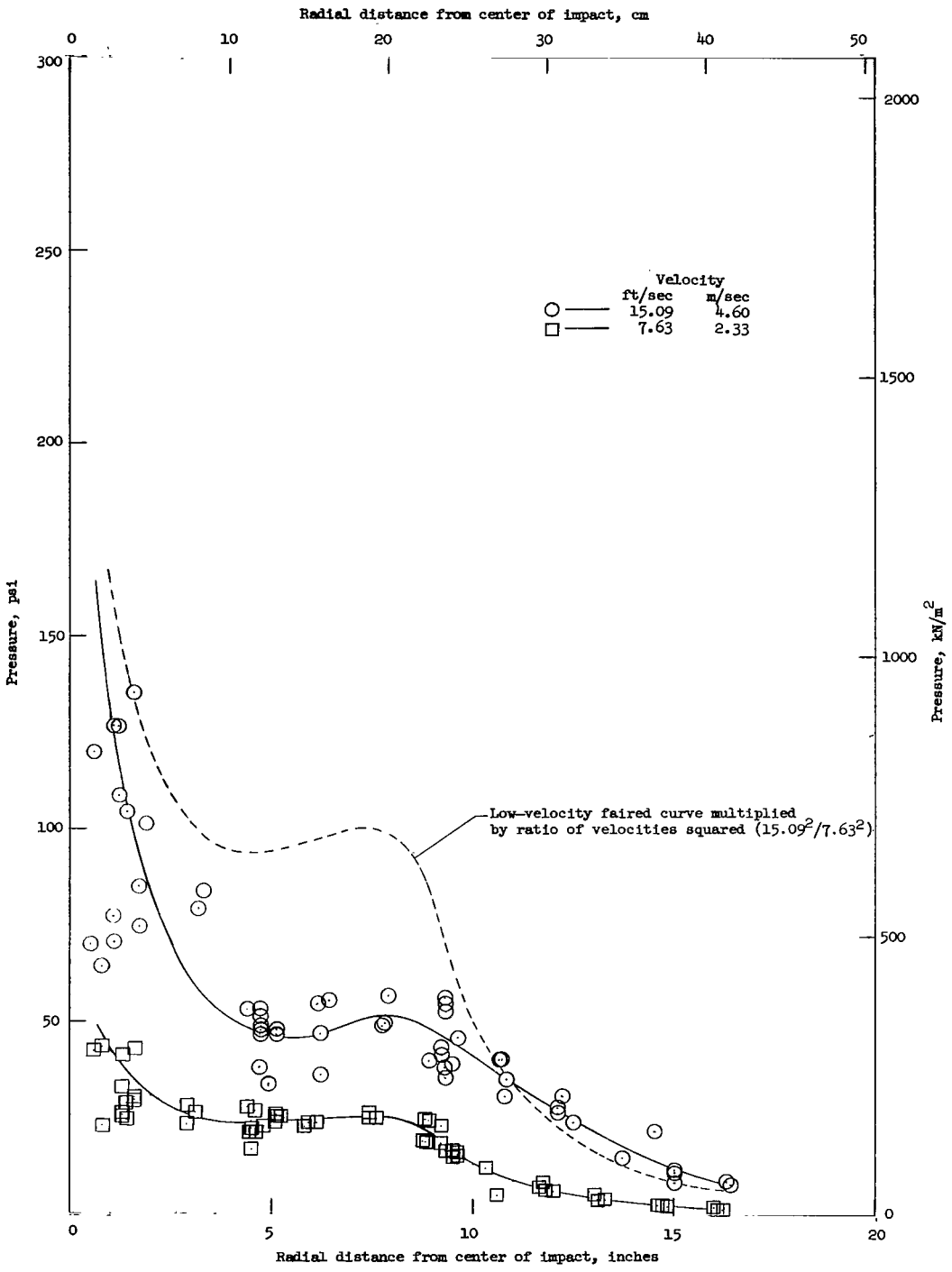

(b) Flexible-bottom model.

Figure 9.- Concluded.

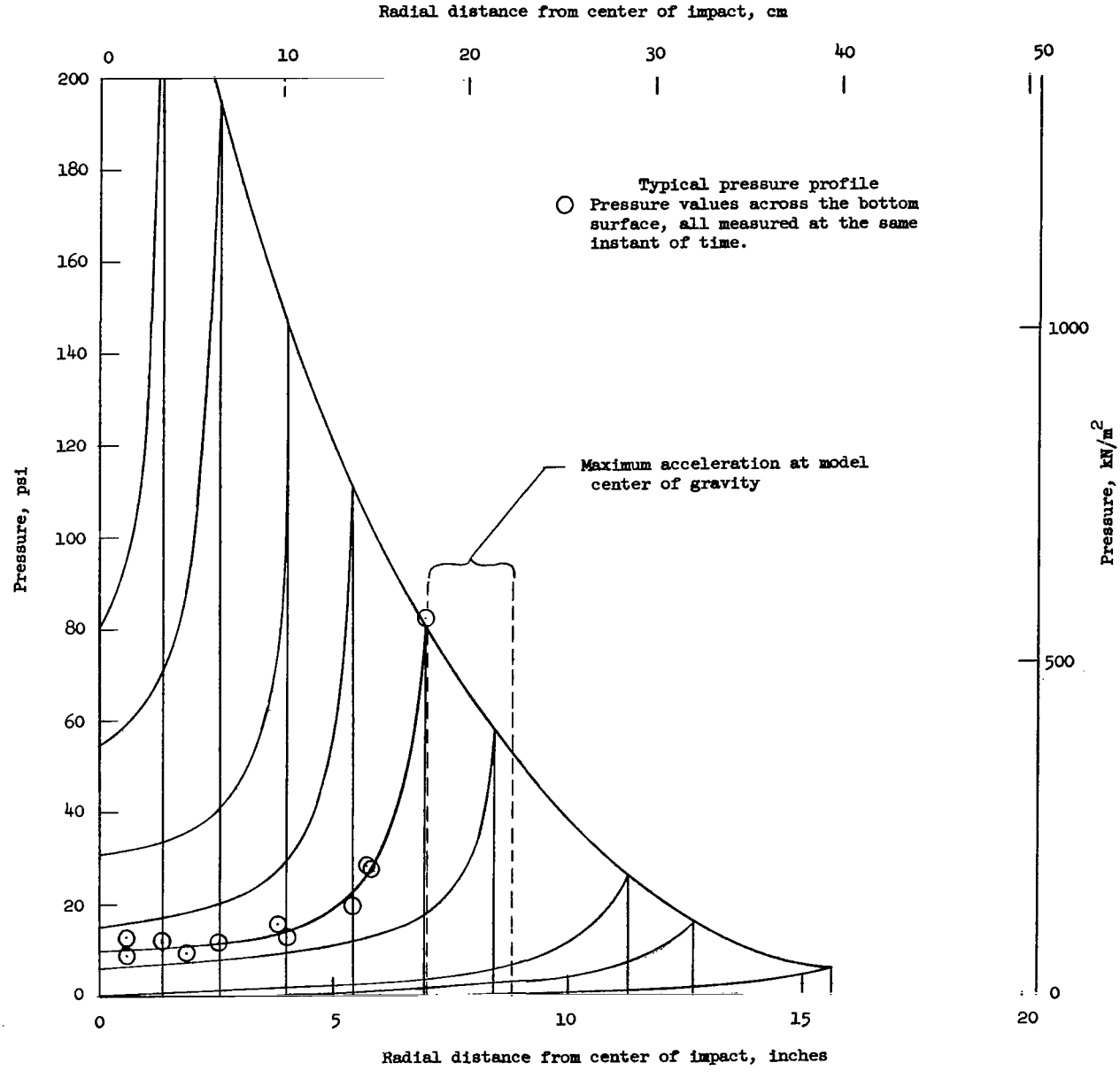

(a) Solid model 2. Run 6; vertical velocity, 15.33 ft/sec (4.67 m/sec).

Figure 10.- Pressure profiles for solid and flexible-bottom models.

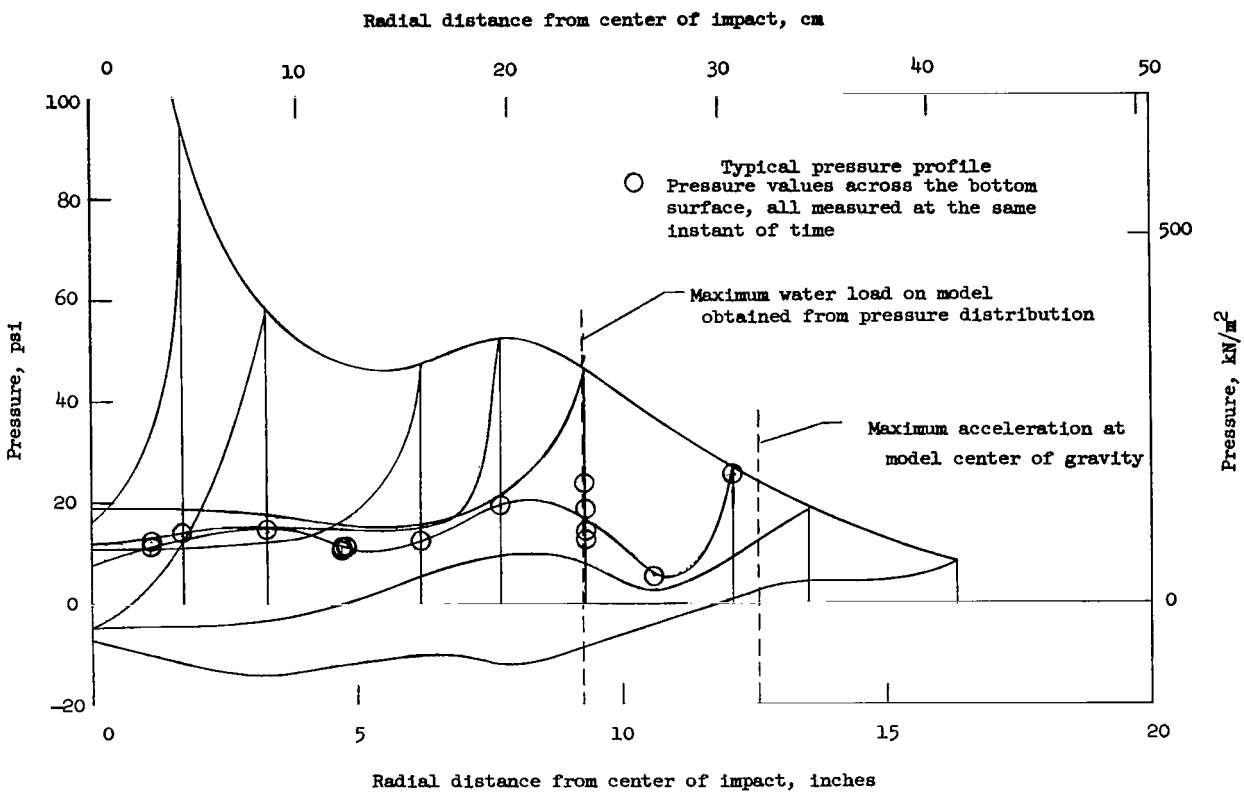

(b) Flexible-bottom model. Run 4; vertical velocity, 15.08 ft/sec (4.60 m/sec).

Figure 10.- Concluded.

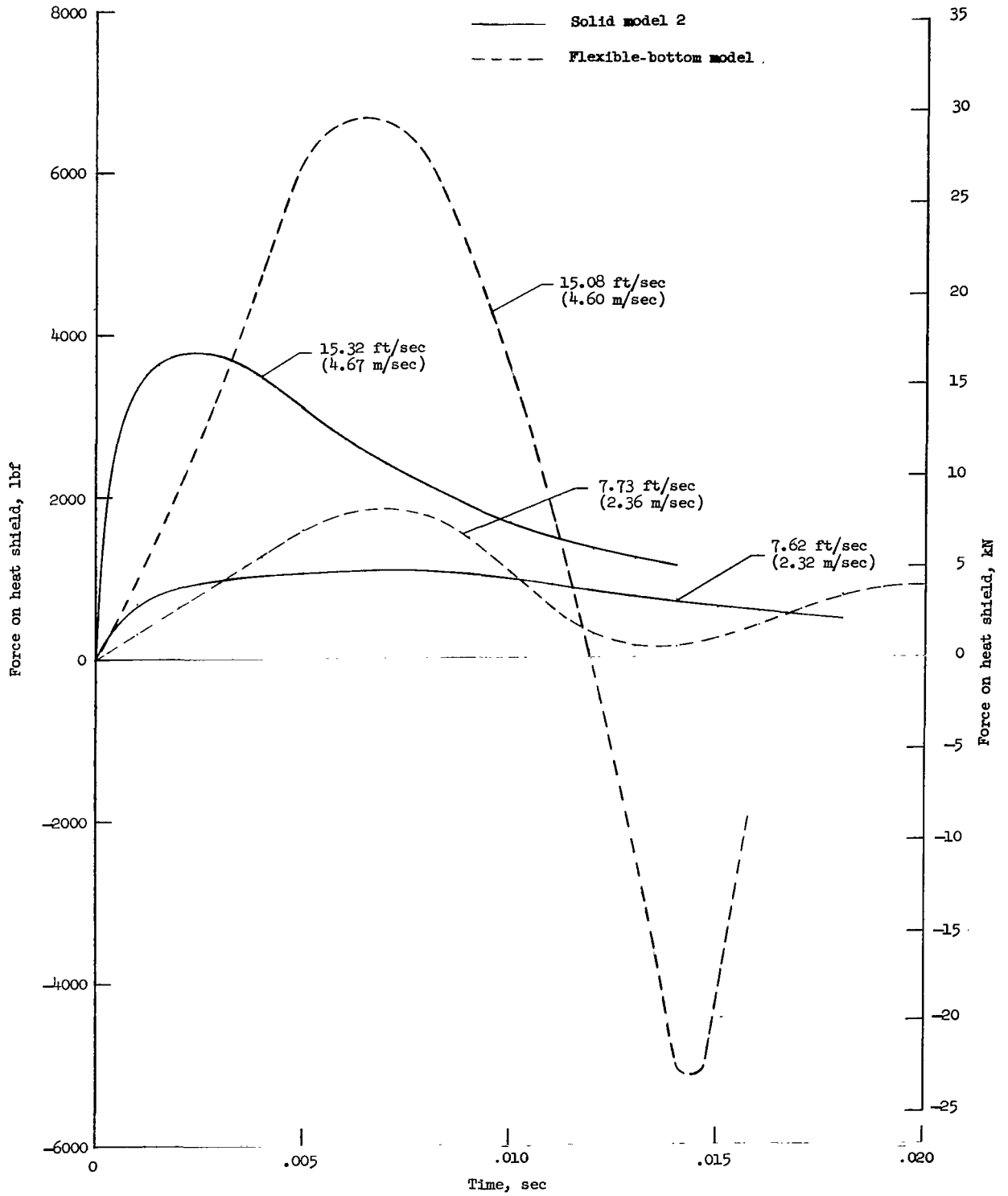

Figure 11.- Comparison curves showing effect of bottom flexibility on the force applied to the bottom.

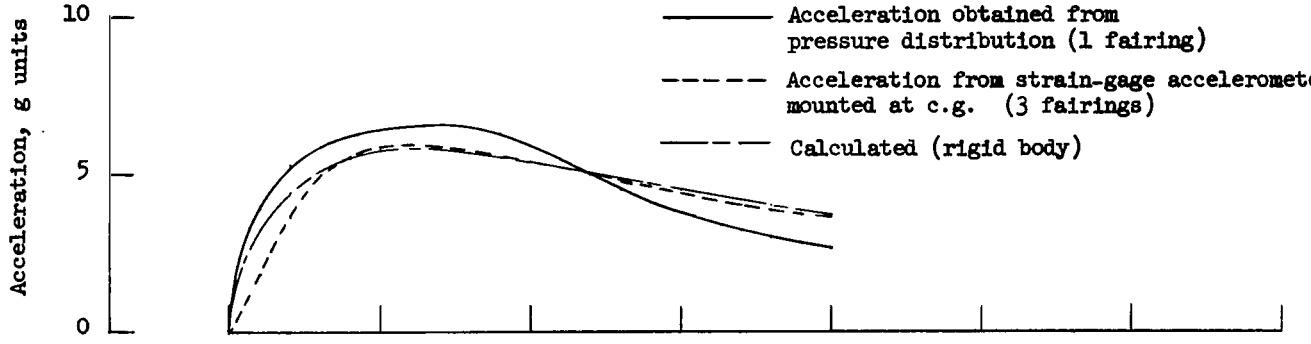

(a) Solid model 2. Run 1; vertical velocity, 7.62 ft/sec (2.32 m/sec).

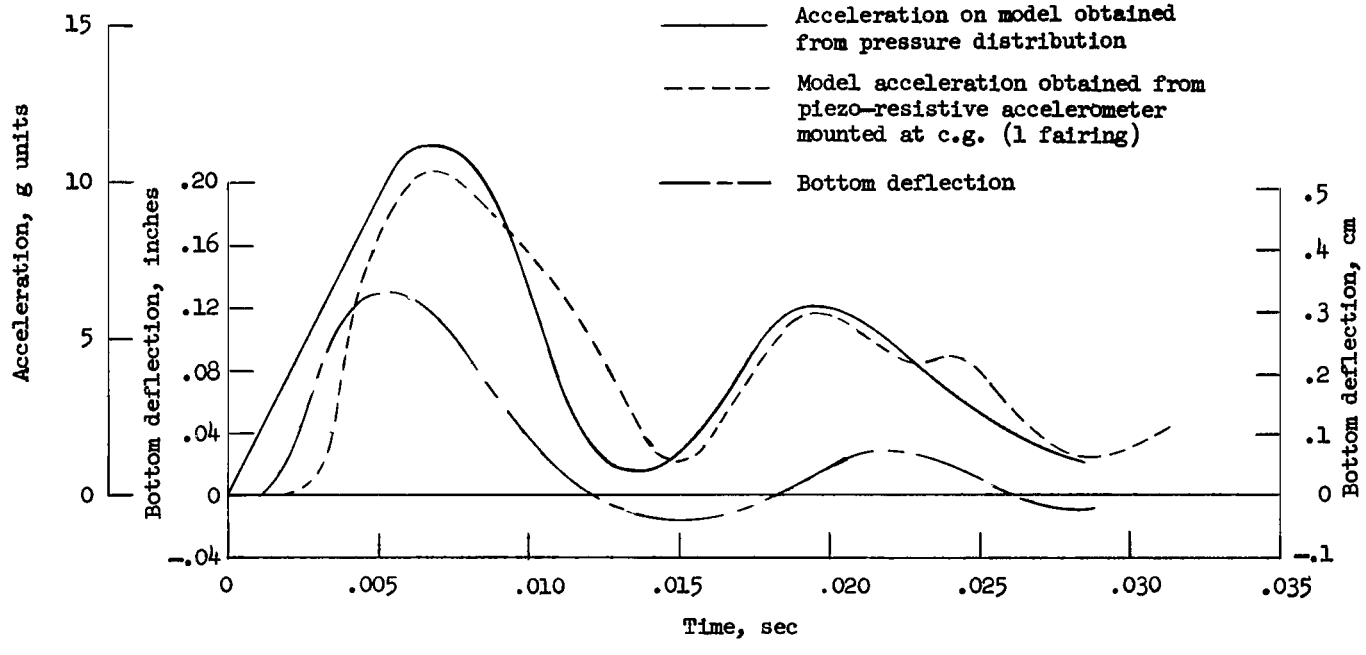

(b) Flexible-bottom model. Run 1; vertical velocity, 7.73 ft/sec (2.36 m/sec).

Figure 12.- Comparison of acceleration and bottom-deflection time histories for low-velocity impacts.

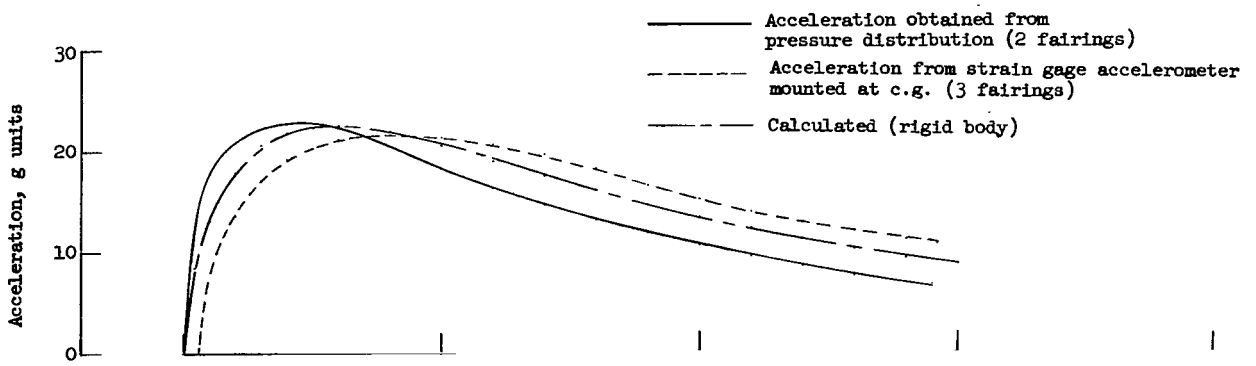

(a) Solid model 2. Run 4; vertical velocity, 15.32 ft/sec (4.67 m/sec).

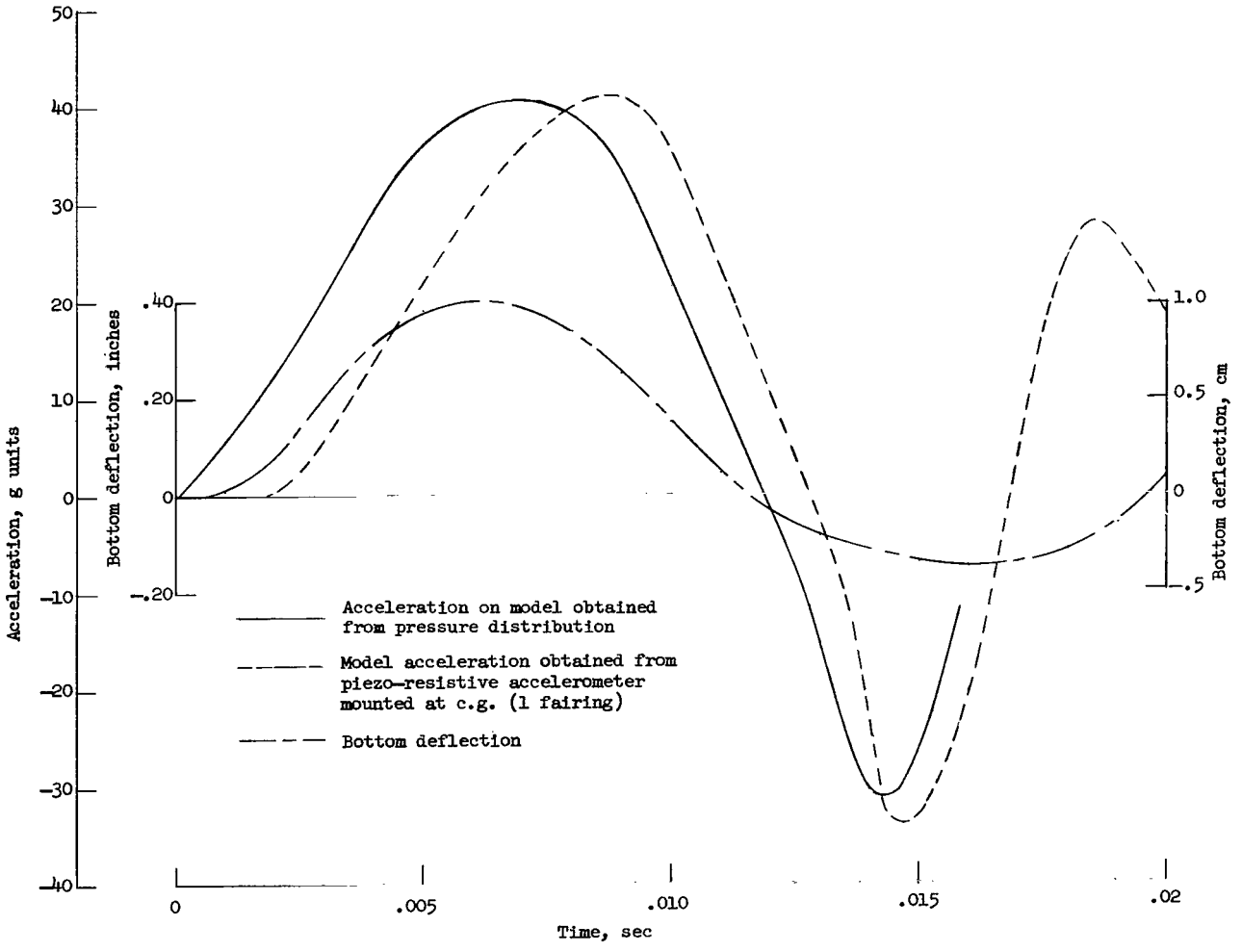

(b) Flexible-bottom model. Run 4; vertical velocity, 15.08 ft/sec (4.60 m/sec).

Figure 13.- Comparison of acceleration and bottom-deflection time histories for high-velocity impacts.

NATIONAL AERONAUTICS AND SPACE ADMINISTRATION
WASHINGTON, D. C. 20546
OFFICIAL BUSINESS

FIRST CLASS MAIL

POSTAGE AND FEES PAID
NATIONAL AERONAUTICS AND
SPACE ADMINISTRATION

POSTMASTER: If Undeliverable (Section 158 Postal Manual) Do Not Return

"The aeronautical and space activities of the United States shall be conducted so as to contribute . . . to the expansion of human knowledge of phenomena in the atmosphere and space. The Administration shall provide for the widest practicable and appropriate dissemination of information concerning its activities and the results thereof."

—NATIONAL AERONAUTICS AND SPACE ACT OF 1958

NASA SCIENTIFIC AND TECHNICAL PUBLICATIONS

TECHNICAL REPORTS: Scientific and technical information considered important, complete, and a lasting contribution to existing knowledge.

TECHNICAL NOTES: Information less broad in scope but nevertheless of importance as a contribution to existing knowledge.

TECHNICAL MEMORANDUMS: Information receiving limited distribution because of preliminary data, security classification, or other reasons.

CONTRACTOR REPORTS: Scientific and technical information generated under a NASA contract or grant and considered an important contribution to existing knowledge.

TECHNICAL TRANSLATIONS: Information published in a foreign language considered to merit NASA distribution in English.

SPECIAL PUBLICATIONS: Information derived from or of value to NASA activities. Publications include conference proceedings, monographs, data compilations, handbooks, sourcebooks, and special bibliographies.

TECHNOLOGY UTILIZATION PUBLICATIONS: Information on technology used by NASA that may be of particular interest in commercial and other non-aerospace applications. Publications include Tech Briefs, Technology Utilization Reports and Notes, and Technology Surveys.

Details on the availability of these publications may be obtained from:

SCIENTIFIC AND TECHNICAL INFORMATION DIVISION

NATIONAL AERONAUTICS AND SPACE ADMINISTRATION

Washington, D.C. 20546